Conformational Ordering in Growing Spherulites of Isotactic Polypropylene

ARTICLE *in* MACROMOLECULES · NOVEMBER 2010

Impact Factor: 5.8 · DOI: 10.1021/ma1019686

9 AUTHORS, INCLUDING:

Zeming Qi
University of Science and Technology of China
97 PUBLICATIONS **1,152** CITATIONS
SEE PROFILE

Liangbin Li
University of Science and Technology of China
137 PUBLICATIONS **2,045** CITATIONS
SEE PROFILE

Macromolecules
ARTICLE

Macromolecules **2010**, *43*, 9859–9864 **9859**
DOI: 10.1021/ma1019686

Conformational Ordering in Growing Spherulites of Isotactic Polypropylene

Yuanhua Cong,[†] Zhihua Hong,[‡] Zeming Qi,[†] Weiming Zhou,[†] Hailong Li,[†] Hao Liu,[‡] Wei Chen,[‡] Xiao Wang,[†] and Liangbin Li*,[†,‡]

[†]*National Synchrotron Radiation Laboratory and College of Nuclear Science and Technology, University of Science and Technology of China, Hefei, China, and* [‡]*Department of Polymer Science and Engineering, CAS Key Lab of Soft Matter Chemistry, University of Science and Technology of China, Hefei, China*

Received August 25, 2010; Revised Manuscript Received October 17, 2010

ABSTRACT: The conformational ordering in spherulites of isotactic polypropylene during growing process is studied with in situ infrared microspectroscopic imaging. A comparison between the intensity distribution of bands representing crystal and conformational ordering indicates that large concentration of conformational ordered segments exist in the growth boundary region of spherulites, which suggests that conformational ordering takes place before packing into crystal lattice in the growth boundary layer. The width of the growth boundary layer is sensitive to temperature but keeps relative constant during isothermal crystallization process. Though the interchain organization of the conformational ordered segments is not clear yet, conformational ordering in the growth boundary layer is assigned to be a preordering step of crystallization.

Introduction

Polymer crystallization is a long-standing challenge of polymer physics, which has been attracting great efforts owing to its fundamental interest and industrial importance, as two-thirds of the industrial polymers are crystallizable. During last 60 years, though different theories or models have been developed to elucidate molecular picture of polymer crystallization, no full agreement is reached yet.[1−10] One crucial issue is whether a preordering stage exists before the onset of crystallization.

Lauritzen-Hoffman (LH) theory[2,3] with nucleation and growth as a stepwise process assumes a direct transition from entangled polymer chains with random coil state to crystal occurring at the growth front without any preordering stages, which has been dominating the discussion of polymer crystallization during last 60 years although criticisms are always accompanied since its establishment. Since 1990s, increasing evidence show that intermediate processes via metastable structures take place during the transformation from the entangled melt to the final crystal.[10−22] A spinodal-assisted process in induction period is concluded from observations with small-angle X-ray scattering (SAXS), depolarized light scattering (DPLS), and Fourier transform infrared (FTIR). The observed orientation fluctuation is considered to be nematic structure which is composed of conformational ordered segments (CORS) in amorphous state before crystallization.[10−16] Olmsteld et al. further developed a more general theory of spinodal assisted-crystallization.[17] During last 10 years, evidence from experiments and computer simulations have been collected to support or oppose this idea.[10−24] Instead of concerning the induction period, Strobl et al. proposed a multistage growth model. A preordered structure is suggested to form at the growth front which transforms to a granular crystal state.[8,9] Evidences from atomic force microscope (AFM),[25] the comparison of crystallization and melting lines and etc., support the multistage process with the existence of preordering.[8,9]

*Corresponding author. E-mail: lbli@ustc.edu.cn.

Though the detailed interchain organizations are different from different models, it is generally accepted that conformational ordering must be a necessary step for both preordering mechanism and nucleation theory.[1−10] Polymer ordering includes intrachain conformational ordering and interchain orientational and positional ordering. The essential difference between crystallization via a preordering step and the traditional view of nucleation and growth model is whether intra- and intermolecular orderings occur in sequence or simultaneously. Ideal crystal requires that all orders are long-range, while preordering structures contain one or two of them in which intrachain conformational ordering seems to be essential. Thus, tracing intrachain conformational ordering is the first step to unveil the complex ordering process of polymer crystallization, which has been conducted by some groups.[26−29] In the induction period, conformational ordering has indeed been observed before the occurrence of crystallization. It is natural to conjecture that conformational ordering should also take place at the growth front of crystal. The existence of conformational ordering may not directly support Strobl's model, but it certainly provides a different view from LH theory. However, directly detecting the conformational ordering at the growth front is a grand challenge, as it requires a spectral method with spatial resolution in nanometers and time resolution in seconds.

In this work, an indirect approach is employed to check the existence of conformational ordering at the growth front, where the conformation ordering and the growth of spherulite are tracked with in situ FTIR microspectroscopic imaging. Instead of detecting the growth front of spherulite, we extract information on conformational ordering inside spherulite as the growth front of spherulite is hard to define. The growth of spherulite proceeds by branching and splaying of the dominant lamellae, which provide the framework of spherulite within which plenty of melt exists. A filling process is followed through a transformation from melt to subsidiary lamellae.[31−34] This kind of geometry sleads to tremendous difficulties in the investigation of the growth

Published on Web 11/12/2010

front of a spherulite as the relative content of dominant lamellae is small. Our approach is to detect whether conformational ordering exists in the melt within the framework of spherulite during the filling process. A comparison between the bands representing crystal and conformational ordering indicates that conformational ordering does occur in the melt within spherulite.

Experimental Section

High-molecular-mass isotactic polypropylene (iPP) used in this study was kindly supplied by SABIC-Europe. It has a melt flow index about 0.3 g/10 min (230 °C/2.16 kg, ASTM D1238) and an average M_n and M_w of about 150 and 720 kg/mol, respectively. The melting point is around 165 °C.

The IR imaging measurement was performed on IR spectroscopy and microspectroscopic imaging endstation at National synchrotron Radiation Laboratory. The endstation equips with a Bruker HYPERION 3000 microscope coupled to Bruker IFS 66v FTIR spectrometer. With a 64 × 64 elements Focal Plane Array (FPA) detector, 250 μm × 250 μm areas can be measured fast. A homemade hot stage with a temperature uncertainty of ±0.1 °C is developed for the in situ experiment.

The iPP film of ca. 200 μm thickness was put onto a ZnSe window and heated up to 210 °C for 10 min to erase possible memory effects. Then the film was cooled to 135 °C to initiate nucleation. Then sample was heated up again to the required temperature for isothermal crystallization and kept for 10 min to reach the stably growing state before growth kinetic test. IR spectra at a resolution of 4.0 cm^{-1} were immediately collected following the snapshot of optical imaging. For all experiments, the measured spectrum wavenumber range was 3900−700 cm^{-1} and 128 scans were taken for averaging. The baseline of spectra was carefully adjusted uniformly using OPUS 5.5 package. Height of peak is considered as integral intensities of the conformational bands in all of IR data in this study.

Results

IR microspectroscopic imaging has been employed to investigate the evolution of helical sequences of iPP with high spatial and time resolution under different isothermal crystallization condition. Herein, two conformational characteristic bands are used for analysis. The one at 1303 cm^{-1} is taken to stand for crystal, as it appears after the onset of crystallization, which has been assigned to helices with 13 monomers.[27,35] The band at 998 cm^{-1} refers to conformational ordering as it exists in melt and increases intensity sharply with the onset of crystallization, which has been assigned to helices with 10 monomers.[27,35] After the onset of crystallization, the intensity of 998 cm^{-1} band is contributed by both crystal and melt. If a preordering including conformational ordering takes place, the intensity of 998 cm^{-1} band also contains the contribution of preordering. For the convenience of description, we define these three contributions as crystal, conformational ordered segments from normal melt ($CORS_m$) and conformational ordered segments from preordering ($CORS_p$).

A typical optical microscope image is shown in Figure 1A, which was caught in an isothermal process at 145 °C (Figure 1A). The corresponding IR spectra were also collected by FPA detector simultaneously. Absorption spectra in Figure 1B are taken from the 64 points marked along a red line in Figure 1A, which covers both melt and spherulitic zones. A series of conformational bands are clearly observed. The bands at 1220, 1167, 1303, 998, 1153, and 973 cm^{-1} correspond to helical structures with degree of order from high to low.[27,28,30,35] 973, 1153, and 998 cm^{-1} bands appear both in melt and the spherulite. 1303, 1167, and 1220 cm^{-1} bands emerge only in spherulitic zone. Intensities of 1153 and 973 cm^{-1} bands are higher in melt zone than those in spherulite. This trend indicates population of short helices decreases in spherulite due to their transformation to longer helices, while the formation of long helices leads to the appearance and

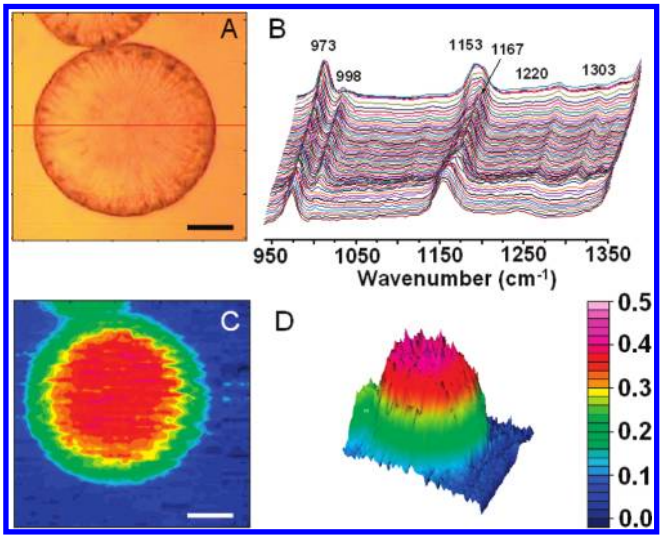

Figure 1. (A) Optical microscope image of two impinged spherulites; (B) Series of IR single spectra at the positions marked along red line in part A. The corresponding contour map (C) and 3-D image of intensity distributions of 998 cm^{-1} band (D), respectively, are given. (The scale bar is 50 μm.)

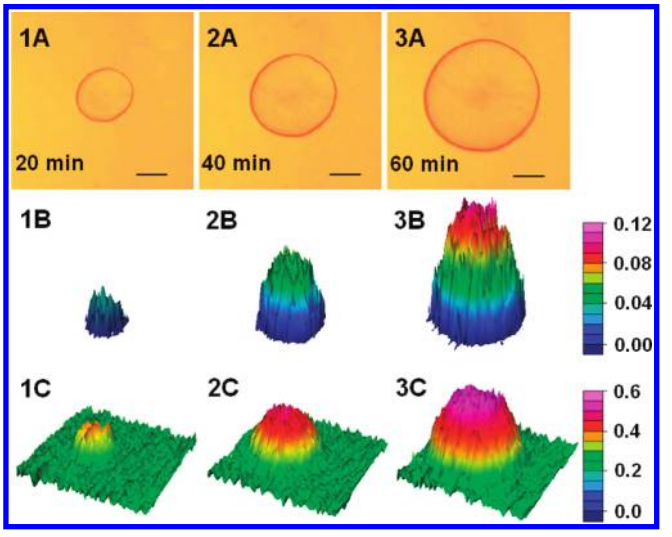

Figure 2. In-situ optical microscope images of a single spherulite (set of A) and the corresponding 3D images of intensity distribution of different conformational bands (Sets of B and C refer to 1303 and 998 cm^{-1} bands, respectively. 1−3 are collected at different times during isothermal crystallization at 142 °C. The scale bar is 50 μm.)

increase of intensities of 1303, 1167, and 1220 cm^{-1} bands. The contour map and 3-dimensional (3D) image of the intensity distribution of 998 cm^{-1} band related to the optical microscope image (Figure 1A) are presented in Figure 1C and 1D, respectively. The change of color from deep blue to pink (Figure 1C) and the increase of height (Figure 1D) reflect the increase of the integral intensity of the conformational band. Clearly, CORS exists in the melt outside spherulite (M_{out}) and increases sharply in spherulite, which is fully in agreement with previous studies about melt crystallization of iPP.[27,28] On the basis of the microspectroscopic imaging, not only the geometry of the spherulites but also the distribution of helices with different orders is unveiled, which demonstrates one of the advantages of IR microspectroscopic imaging for this study.

Optical microscope images (set of A in Figure 2) exhibit the kinetic progress of a growing spherulite at 142 °C. The corresponding in situ IR spectra are also collected. After the imaging

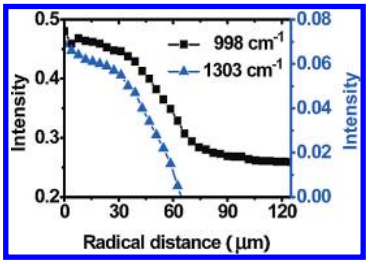

Figure 3. Intensity distributions of 998 cm^{-1} (black squares) and 1303 cm^{-1} (blue triangles) bands against radial distance x.

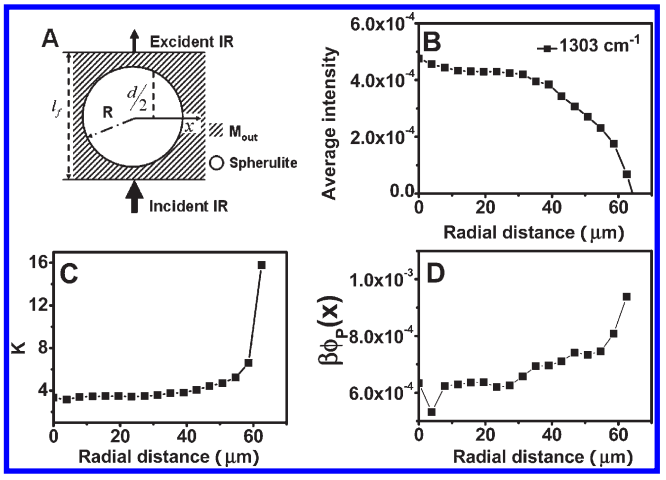

Figure 4. (A) Lateral sectional scheme of a growing spherulite embedded in melt matrix; (B) average intensity of 1303 cm^{-1} in unit height $(I_{1303}(x)/2(R^2 - x^2)^{1/2})$ vs radial distance; (C) K vs radial distance; (D) $\beta\phi_P(x)$ vs radial distance calculated from Figure 3.

technique treatment, the spatial distribution of intensities of 998 cm^{-1} (set of C) and 1303 cm^{-1} (set of B) bands are presented in Figure 2 as 3D images. The intensity of 998 cm^{-1} band in melt zone keeps relatively constant during the whole crystallization process, which is obviously weaker than that in the spherulitic zone. Comparing the kinetic process of 998 cm^{-1} band with optical microscope images, it is clear that 998 cm^{-1} band is more sensitive to reflect the growth of spherulite. Intensity of 998 cm^{-1} band gradually increases in both the boundary and the central zones, which are attributed to the expansion of dominant lamellae and filling process, respectively. The signal of 1303 cm^{-1} can only be resolved inside the growing spherulite, which is also consistent with the early studies on melt crystallization of iPP with normal FTIR.[27,28] The different spatial distributions of the intensities of 998 cm^{-1} and 1303 cm^{-1} bands reflect the distribution of different degrees of orders during the growth of spherulite.

In order to quantitatively analyze the distribution of conformational ordering and crystallization, we calculate the average intensities of 998 and 1303 cm^{-1} against the radial distance x of the spherulite. The results of 2B and 2C in Figure 2 collected at 142 °C are taken as an example which is shown in Figure 3. The center of spherulite has the highest intensity of 998 cm^{-1} band, which decreases with the increase of radial distance and reaches a plateau in the melt zone. Accordingly, the intensity evolution of 1303 cm^{-1} band gives the similar trend as 998 cm^{-1} band. The intensity evolution is ascribed to two factors. (I) Geometric factor: the thickness of the spherulite in the vertical direction decreases via a circle function against the radius as illustrated in Figure 4a. (II) Structural factor: the crystallinity decreases along the radial axis due to the filling process. Our concern is the structural factor (II), namely the crystallinity and conformational ordering in the filling process. Thus, we first eliminate the geometric factor (I). The geometry of target spherulite is an approximately regular sphere in the test iPP film. Through a simple geometric calculation, we have

$$d = 2\sqrt{R^2 - x^2}$$

the thickness of the crystallized zone, where R refers to the radius of the spherulite and x is the radial distance in horizontal direction as marked in Figure 4A. According to the Beer−Lambert law, the absorbance is directly proportional to thickness of a sample. Thus, the geometric factor (I) can be corrected with absorbance dividing the corresponding thickness. After the geometric correction, the variation of absorption intensity can be solely attributed to structural factor.

The intensity of 1303 cm^{-1} band in unit height $(I_{1303}(x)/2(R^2 - x^2)^{1/2})$ is plotted against radial distance x in Figure 4B, where $I_{1303}(x)$ is the intensity of 1303 cm^{-1} band as a function of radial distance x from Figure 3. The value of $I_{1303}(x)/2(R^2 - x^2)^{1/2}$ shows a relative flat region and then decreases sharply with the increase of radial distance x, which reflects the average content of crystal in unit height. In other word, the crystallinity in unit height keeps relatively constant with $x < 30\,\mu$m and decreases sharply at larger radial distance x.

After estimating the crystal distribution through the intensity of I_{1303}, we come to calculate the content of CORS through the intensity of 998 cm^{-1} band. The total absorption intensity of 998 cm^{-1} band ($I_{998-total}(x)$, see Figure 3) is contributed by crystal and CORS inside and outside spherulite (M_{in} and M_{out} stand for the melt inside and outside spherulite, respectively.) (as illustrated in Figure 4A). Denoting the film thickness as l_f, the thickness of M_{out} is $l_f - 2(R^2 - x^2)^{1/2}$. Focusing on the absorption from spherulitic zone, the contribution by M_{out} can be removed as:

$$I_{998}(x) = I_{998-total}(x) - I_{A0}(l_f - 2\sqrt{R^2 - x^2}) \quad (1)$$

In left side of eq 1, $I_{998}(x)$ is the absorption intensity of 998 cm^{-1} band from the spherulitic zone. The second term in the right side is the absorption intensity of M_{out}. I_{A0} stands for the absorption intensity per unit height of 998 cm^{-1} in melt, which can be measured at the position without crystal on the same sample and at the same conditions. If no any preordering takes place, $I_{998}(x)$ is contributed by $CORS_m$ in M_{in} and crystal. Without preordering the concentrations of $CORS_m$ in the M_{in} and M_{out} are the same and $I_{998}(x)$ can be formulated as follows:

$$I_{998}(x) = I_{C-998}(x) + I_{A0}2\sqrt{R^2 - x^2}[1 - \phi_C(x)] \quad (2)$$

where $I_{C-998}(x)$ is the absorption intensity contributed by crystal, which is proportional to $I_{1303}(x)$ since both $I_{C-998}(x)$ and $I_{1303}(x)$ originate from the same crystal. Thus, their relationship can be written as $kI_{1303}(x) = I_{C-998}(x)$, where k is a constant. $\phi_C(x)$ is the crystallinity which is also varied with radial distance x and can be expressed as

$$\phi_C(x) = \frac{kI_{1303}(x)}{I_{C0}2\sqrt{R^2 - x^2}}$$

I_{C0} means the absorption of 998 cm^{-1} band per unit height of crystal. K is defined as $K = k(1 - \alpha)$, where $\alpha = I_{A0}/I_{C0}$. As k, I_{C0} and I_{A0} all are constants, $K = k(1 - \alpha)$ should be a constant too. On the basis of eq 2, K is given by:

$$K = \frac{I_{998}(x) - I_{A0}2\sqrt{R^2 - x^2}}{I_{1303}(x)} \quad (3)$$

in the case when no preordering takes place.

Figure 4C plots of K vs radial distance x. K slowly goes up with the increase of radial distance x first, which rises sharply near the

boundary of spherulite. The deviation of K from a constant is due to the assumption that no preordering takes place inside spherulite, and M_{in} and M_{out} have the same concentration of CORS. The increase of K along radial distance x suggests $M_{in} > M_{out}$ and extra CORS or preordering structure (defined as $CORS_p$ before) exists within spherulite. Considering the contribution by $CORS_p$, eq 2 is modified as follows:

$$I_{998}(x) = I_{C-998}(x) + I_{A0}2\sqrt{R^2 - x^2}[1 - \phi_C(x) - \phi_P(x)] + I_{P0}2\sqrt{R^2 - x^2}\phi_P(x) \quad (4)$$

where the last term at right side of eq 4 is directly contributed by $CORS_p$. $\phi_P(x)$ is the relative concentration of $CORS_p$ and I_{P0} is the absorption intensity of $CORS_p$ per unit height. To obtain $\phi_P(x)$ directly, eq 4 is expressed as:

$$\beta\phi_P(x) = \frac{(K' - K)I_{1303}(x)}{2\sqrt{R^2 - x^2}} \quad (5)$$

where $K = k(1-\alpha)$ is constant.

$$K' = \frac{I_{998}(x) - I_{A0}2\sqrt{R^2 - x^2}}{I_{1303}(x)}$$

varies with radial distance x, which can be calculated from Figure 3 directly. Though the expression of K' is the same as that of K, the definition of K' is at the situation that preordering occurs. As $\beta = (I_{P0} - I_{A0})$ is constant, $\beta\phi_P(x)$ represents the concentration of $\phi_P(x)$ directly. As K is not available directly at this moment, the value K given by eq 3 is carefully selected from our experimental data. We take $K = 2.0$ to calculate the evolution of $\beta\phi_P(x)$ along with radial distance x and plot in Figure 4D. This K value is estimated with eq 3 at the central region of the spherulite crystallized at 135 °C, which gives the lowest K value in this work and has the lowest content of $CORS_p$. This K value is also the closest to the real K value. The evolution of $\beta\phi_P(x)$ indicates the existence of $CORS_p$ within the spherulite, which increases with radial distance x.

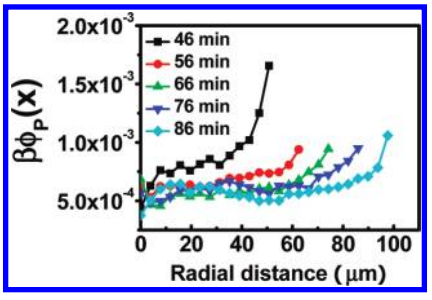

Figure 5. Series of $\beta\phi_P(x)$ vs radial distance curves at different crystallization time during isothermal process at 142 °C.

Following the same data treatment procedure in Figure 4, we analyze the content of $CORS_p$ during isothermal crystallization process at different crystallization time at 142 °C, which is presented in Figure 5. All $\beta\phi_P(x)$ curves show similar trend, which increases slightly with x in the central region of spherulite and has a sharply level-up at the growth boundary of spherulite. The average level-up zones during the isothermal crystallization process keep relative constant of about 20 μm, which suggests that the growth boundary with large content of $CORS_p$ is an intrinsic character of polymer crystallization. The average $\beta\phi_P(x)$ in the center of spherulite decreases slightly with crystallization time.

We further check the evolution of $\beta\phi_P(x)$ at different crystallization temperatures. In order to obtain spherulites with similar size, the isothermal crystallization times at different temperatures are different, which are 12, 38, 46, 70, and 167 min at temperature of 135, 140, 142, 145, and 150 °C, respectively. Spectra from spherulites growing isothermally at different temperatures with similar size are collected and analyzed using the same methods. The plots of $\beta\phi_P(x)$ vs radial distance x show similar trend as that at 142 °C, which are presented in Figure 6A. However, $\beta\phi_P(x)$ in the central region of spherulites varies with temperature, which does not follow a monotonic trend. In the central region of spherulite, $\beta\phi_P(x)$ is the largest at 142 °C, while both higher and lower temperatures give a lower value of $\beta\phi_P(x)$. The average values of $\beta\phi_P(x)$ near the center of spherulite are plotted against temperature in Figure 6B, which gives a direct indication on the relative content of $CORS_p$ in spherulites crystallized at different temperatures.

Discussion

The evolution of $\beta\phi_P(x)$ during isothermal crystallization process at various temperatures (Figures 5 and 6) suggests the existence of CORSp, which leads to the content of CORS in M_{in} is larger than that in M_{out} per unit height. In another word, in addition to crystallization, extra CORS exists inside spherulite. We will first discuss the origin of this extra conformational ordering, and then try to construct a molecular picture on the growth of spherulite or lamellar crystals.

Related to crystallization, the extra conformational ordering inside spherulite can be either a consequence of crystallization or a prestep or preordering of crystallization. It is no doubt that crystallization will induce conformational ordering in the melt around lamellar crystals. The long-chain nature of polymers lead to a unique crystal growth fashion, during which one single chain can pack portion of chain into crystal lattice, while leaves rest part in the melt. At the end, the single chain goes through several lamellar crystals and interlamellar amorphous regions. This growth fashion creates entangled polymer brush if we take the lamellar crystal as substrate. On the basis of either early Zachmann's calculation[36] on the surface model of lamellar nuclei or theory on the

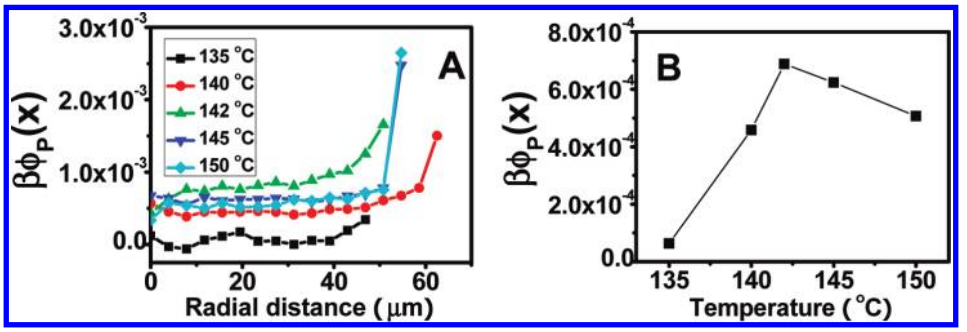

Figure 6. (A) Series of $\beta\phi_P(x)$ vs radial distance curves in isothermal process at different temperatures. (B) Average values of $\beta\phi_P(x)$ near the central region of spherulites against temperature.

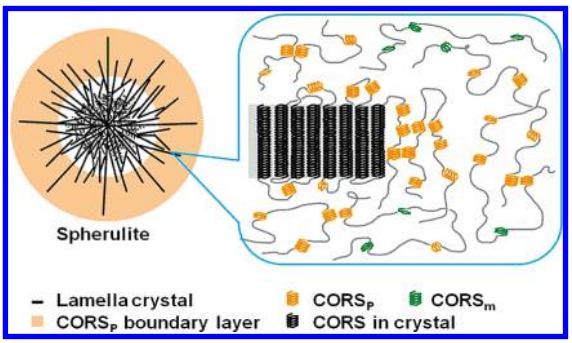

Figure 7. Schematic illustration of a growing spherulite with boundary layer containing large concentration of conformational ordered segments.

conformation of crowded brush,[37,38] chains with fixed end will lose freedom or entropy, which corresponds to conformational ordering. The reeling force introduced in LH theory leads to the same conclusion, as stretching chain to a larger end-to-end distance increases the content and the length of CORS.[2,3] Thus, interlamellar amorphous should have higher content of CORS than that outside spherulite, which even leads to the concept of rigid amorphous.[39] Thus, crystallization induced conformational ordering around lamellar crystals certainly exists during crystallization process, which may also be defined as a prestep or preordering for crystallization.

If all the extra conformational ordering in the melt around lamellar crystals is originated from the brush model, we would expect the concentration of CORS$_p$ in the melt is proportional to the crystallinity, which, however, does not consist with the above results. In the central region of the spherulite, the average crystallinity is certainly higher than that in the boundary region, as a filling process of subsidiary lamellae happens during the growth of spherulite. After corrected by the geometric factor, the intensity of 1303 cm^{-1} in Figure 4B clearly supports the spherulitic picture with higher crystallinity in the central region. In contrast, results in Figure 5 and Figure.6 show $\beta\phi_P(x)$ increases with radial distance x and has a sharp level-up in the boundary region of the spherulite, which indicates that the boundary region of spherulite has higher volume fraction of CORS$_p$ than that in the center. A direct conclusion is that preordering does not correlate with the concentration of lamellar crystals. Thus, in addition to the contribution of the brush model discussed above, a true preordering takes place in the growth boundary region of spherulite.

The evolution of $\beta\phi_P(x)$ along with radial distance x suggests the boundary region of growing spherulite contains high concentration of CORS$_p$ or preordering. This conclusion is also supported by the results on the growth at different crystallization time and temperatures (see Figure 5 and 6). A schematic illustration of a growing spherulite is presented in Figure 7, where a boundary layer with high concentration of CORS$_p$ or preordering is highlighted with yellowish-brown color.

There are two transformation processes in the supercooled melt: the formation of CORS$_p$ and the transition from CORS$_p$ to crystal, thus the width of the boundary layer depends on the competition between the rate of formation of CORS$_p$ (I_{cor}) and the transition from CORS$_p$ to crystal (I_{cry}). In another word, the width of the boundary layer depends on $\Delta I = I_{cor} - I_{cry}$ rather than individual rate alone. Though both rates increase with the decrease of crystallization temperature or increase of supercooling ΔT, they have different temperature dependence. The formation of CORS$_p$ starts at lower supercooling ΔT than crystallization does, while upon decreasing temperature I_{cry} increases faster than I_{cor} does. At temperatures higher than 142 °C, though I_{cry} is slow, I_{cor} is also slow, which keeps ΔI at a low level and leads to a thinner boundary layer. On the other hand, at temperatures lower than 142 °C, though I_{cor} increases, I_{cry} is even accelerated more, as implied by fast crystallization rate. This also leads to a low concentration of CORS$_p$ (a thinner boundary layer). The competition between I_{cry} and I_{cor} results into a maximum of ΔI (at 142 °C) along with the decrease of crystallization temperature (see Figure 6B). This can also explain the reduction of $\beta\cdot\phi_P(x)$ at the central region of the spherulite. As illustrated in Figure 7, the boundary layer covers the whole spherulite, $\beta\phi_P(x)$ is an averaged value over the spherulite height $2(R^2 - x^2)^{1/2}$. As the boundary layer has high concentration of CORS$_p$, the averaged value $\beta\phi_P(x)$ is determined by the relative thickness between the boundary layer and the central region of the spherulite. During the growth process, the boundary layer keeps a relative constant thickness and the central region of spherulite grows with time, which reduces the weight factor of the boundary layer and leads to a decrease of $\beta\phi_P(x)$.

As IR spectroscopy method is only sensitive to intramolecular conformational ordering of iPP, we can only draw a conclusion that the existence of the boundary layers with large content of CORS$_p$ in the growing spherulites. The current results did not provide any evidence on the intermolecular organization of these CORS$_p$. If these CORS$_p$ pack parallel at the growth front of lamellar crystal, it will be the model proposed by Strobl.[8,9] This can be highly possible, as stabilization of high concentration of CORS$_p$ requires extra interactions and intermolecular ordering can be a good source. On the other hand, if the parallel packed CORS$_p$ domains locate around the top and bottom surface, it may be the starting points for subsidiary lamellae. This may explain the branching mechanism during the growth of spherulite, where some subsidiary lamellae do not have any direct contact with dominant lamellae at all.[32]

Conclusions

With in situ IR microspectroscopic imaging technique, conformational ordering at the growth front of spherulite of iPP is studied during isothermal crystallization process at different temperatures. Comparing the intensity distribution of bands representing crystals and CORS, a boundary layer with high concentration of CORS is observed around the growth front of spherulite, whose thickness is determined by the competition between the rates of preordering and its transformation to crystal. As the concentration of CORS in the boundary layer is not correlated with local crystallinity, conformational ordering in this layer may represent a true preordering of crystallization, though the interaction among these CORS is not clear yet.

Acknowledgment. The authors thank Prof. Gert Strobl (Freiburg) and Prof. Wenbing Hu (Nanjing) for fruitful discussion. This work is supported by the National Natural Science Foundation of China (51033004, 50973103, 20774091, 20904050), the Fund for One Hundred Talent Scientist of CAS, 973 program of MOST (2010CB934504), and the experimental fund of NSRL. The research is also in part supported by the State Key Laboratory of Polymer Physic and Chemistry (Changchun Institute of Applied Chemistry, CAS) and the Opening Project of the State Key Laboratory of Polymer Materials Engineering (Sichuan University KF201001)

References and Notes

(1) Li, L. B.; De Jeu, W. H. *Adv. Polym. Sci.* **2005**, *181*, 75–120.
(2) Point, J. J.; Rault, J.; Hoffman, J. D.; et al. *Faraday Discuss.* **1979**, *68*, 365–490.
(3) Hoffman, J. D.; Miller, R. L. *Polymer* **1997**, *38*, 3151–3212.
(4) Sadler, D. M.; Gilmer, G. H. *Phys. Rev. Lett.* **1986**, *56*, 2708–2711.
(5) Cheng, S. Z. D.; Li, C. Y.; Zhu, L. *Eur. Phys. J. E* **2000**, *3*, 195–197.
(6) Lotz, B. *Eur. Phys. J. E* **2000**, *3*, 185–194.
(7) Muthukumara, M. *Eur. Phys. J. E* **2000**, *3*, 199–202.
(8) Strobl, G. *Eur. Phys. J. E* **2000**, *3*, 165–183.

(9) Strobl, G. *Prog. Polym. Sci.* **2006**, *31*, 398–442.
(10) Kaji, K.; Nishida, K.; Kanaya, T.; et al. *Adv. Polym. Sci.* **2005**, *191*, 187–240.
(11) Imai, M.; Kaji, K.; Kanaya, T. *Macromolecules* **1994**, *27*, 7103–7108.
(12) Matsuba, G.; Kaji, K.; Nishida, K.; Kanaya, T.; Imai, M. *Macromolecules* **1999**, *32*, 8932–8937.
(13) Matsuba, G.; Kanaya, T.; Saito, M.; Kaji, K.; Nishida, K. *Phys. Rev. E* **2000**, *62*, R1497–1500.
(14) Ryan, A. J.; et al. *Faraday Discuss.* **1999**, *112*, 13–29.
(15) Heeley, E. L.; Poh, C. K.; Li, W.; Maidens, A.; Bras, W.; Dolbnya, I. P.; Gleeson, A. J.; Terrill, N. J.; Fairclough, J. P. A.; Olmsted, P. D.; Ristic, R. I.; Hounslow, M. J.; Ryan, A. J. *Faraday Discuss.* **2003**, *122*, 343–361.
(16) Heeley, E. L.; Maidens, A. V.; Olmsted, P. D.; Bras, W.; Dolbnya, I. P.; Fairclough, J. P. A.; Terrill, N. J.; Ryan, A. J. *Macromolecules* **2003**, *36*, 3656–3665.
(17) Olmsted, P. D.; et al. *Phys. Rev. Lett.* **1998**, *81*, 373–376.
(18) Gee, R. H.; Lacevic, N.; Fried, L. E. *Nat. Mater.* **2006**, *5*, 39–43.
(19) Hu, W.; Frenkel, D.; Mathot, V. B. F. *Macromolecules* **2003**, *36*, 8178–8183.
(20) Muthukumar, M. *Adv. Polym. Sci.* **2005**, *191*, 241–274.
(21) Yamamoto, T. *Polymer* **2004**, *45*, 1357–1364.
(22) Soccio, M.; Nogales, A.; Lotti, N.; Munari, A.; Ezquerra, T. A. *Phys. Rev. Lett.* **2007**, *98*, 037801.
(23) Hsiao, B. S.; et al. *Macromolecules* **1995**, *28*, 6931–6936.
(24) Wang, W.; Schultz, J. M.; Hsiao, B. S. *Macromolecules* **1997**, *30*, 4544–4550.
(25) Magonov, S.; Godovsky, Y. *Am. Lab.* **1999**, *31*, 52–58.
(26) Kimura, T.; et al. *J. Polym. Sci., B: Polym. Phys* **1998**, *36*, 1227–1233.
(27) Zhu, X. Y.; Yan, D. Y.; Fang, Y. P. *J. Phys. Chem. B* **2001**, *105*, 12461–12463.
(28) An, H. N.; Zhao, B. J.; Ma, Z.; Shao, C. G.; Wang, X.; Fang, Y. P.; Li, L. B.; Li, Z, M. *Macromolecules* **2007**, *40*, 4740–4743.
(29) Geng, Y.; Wang, G. L.; Cong, Y. H.; Bai, L. G.; Li, L. B.; Yang, C. L. *Macromolecules* **2009**, *42*, 4751–4757.
(30) An, H. N.; Li, X. Y.; Geng, Y.; Wang, Y. L.; Wang, X.; Li, L. B.; Li, Z. M.; Yang, C. L. *J. Phys. Chem. B* **2008**, *112*, 12256–12262.
(31) Bassett, D. C. *Principles of Polymer Morphology*; Cambridge Univ Press: Cambridge, U.K., 1981.
(32) Li, L.; Chan, C. M.; et al. *Macromolecules* **2001**, *34*, 316–325.
(33) Hobbs, J. K.; et al. *Polymer* **1998**, *39*, 2437–2446.
(34) Kolb, R.; Wutz, C.; Stribeck, N.; Von Krosigk, G.; Riekel, C. *Polymer* **2001**, *42*, 5257–5266.
(35) Zerbi, G.; Ciampelli, F.; Zamboni, V. *J. Polym. Sci.* **1963**, *C7*, q141–151.
(36) Zachmann, H. G. *Kolloid Z. Z. Polym.* **1969**, *231*, 504–534.
(37) Alexander, S. *J. Phys.* (*Paris*) **1977**, *38*, 983–987.
(38) De Gennes, P. G. *Macromolecules* **1980**, *13*, 1069–1075.
(39) Menczel, J.; Wunderlich, B. *J. Polym. Sci., Polym. Lett. Ed.* **1981**, *19*, 261–264.